Na_xAu and Cs_xAu bimetal clusters: Finite size analogs of sodium–gold and cesium–gold compounds

Ueli Heiz
Institut de Physique Expérimentale, Université de Lausanne, CH-1015 Lausanne, Switzerland

Arthur Vayloyan and Ernst Schumacher
Institute of Inorganic and Physical Chemistry, University of Bern, CH-3000 Bern 9, Switzerland

Chahan Yeretzian[a)]
Institut für Physikalische und Theoretische Chemie, Technische Universität München, D-85748 Garching, Germany

Mauro Stener, Philip Gisdakis, and Notker Rösch
Lehrstuhl für Theoretische Chemie, Technische Universität München, D-85748 Garching, Germany

(Received 14 May 1996; accepted 25 June 1996)

Mixed metal clusters of sodium and cesium with gold have been generated in a supersonic expansion from the mixed vapor phase. Their tendency towards binary cluster formation, relative thermodynamic stability, and ionization potentials have been experimentally and computationally investigated. The properties of the Na_xAu clusters may be understood within an electronic shell model based on delocalized cluster orbitals, whereas the characteristics of Cs_xAu are indicative of substantial ionic interactions. Relativistic density functional calculations have been performed to elucidate the cluster electronic structure and to rationalize observed properties which may not be accounted for by the jellium model. The properties of these finite-size clusters are shown to be related to the known bulk intermetallic compounds sodium–gold and cesium–gold (cesium aurid), respectively. © *1996 American Institute of Physics.* [S0021-9606(96)01837-5]

I. INTRODUCTION

One of the goals of cluster science is to identify unifying concepts of matter at the molecular and the bulk limit. One hopes that the microscopic approach to understand macroscopic phenomena will help separating local from collective contributions to properties of bulk materials.[1] The aim of this study is to specifically address these questions for one particular class of clusters—the bimetal clusters—and to relate cluster characteristics to the properties of the corresponding intermetallic compounds.

Over the last 30 years many fascinating structural and unusual electronic properties have been found in intermetallic phases.[2–5] Among other materials, stoichiometric 1:1 alkali–gold compounds have attracted particular attention.[6–8] Proceeding through the alkali metal series from LiAu to CsAu, a metal-insulator transition occurs upon going from KAu to RbAu.[9,10] Solid CsAu is known to be a semiconductor with an indirect band gap of 2.6 eV.[11] The formation of the gap can only be modeled if relativistic effects are included in a band structure calculation.[12] In addition, this solid is found to have strong ionic character with gold being the negative ion. This appreciable charge transfer from cesium to gold is attributed to the large difference in electron affinity of the two elements.[13] Also of interest are the structural properties of alkali–gold compounds. RbAu and CsAu adopt the octo-coordinated CsCl structure,[7,14] analogous to ionic CsBr or CsI crystals, whereas the structures of the metallic NaAu and KAu are more complicated and still not fully elucidated.[9,10,15,16] While all of these compounds are stable, the heat of formation decreases from LiAu to CsAu.[10] CsAu can only be prepared in high vacuum[7] and is extremely sensitive to oxygen and moisture.[17]

Considering the very characteristic properties and trends reported for alkali–gold compounds, we set out to investigate their finite-size analogs, the alkali/gold bimetal clusters. Here, we focus on monogold alkali clusters, M_xAu. Two systems were selected which, at the bulk limit, lie either clearly on the metallic (Na/Au) or on the ionic (Cs/Au) side of the metal–nonmetal transition (MNMT). The motivation for this research pertains to fundamental and material science oriented aspects. The study of theoretically tractable, small, and isolated bimetal clusters should shed light onto the nature of heterometal bonding. In the long run, these kinds of studies are expected to lead to a deeper understanding of the electronic and structural properties of intermetallic compounds and liquid alloys such as their ionicity and local order.[18] Furthermore, the single gold atom acts as a well defined perturbation to the alkali cluster and allows one to test the range of applicability of the electronic shell model for metal clusters. Finally, highly stable bimetal clusters are potentially important building blocks for future cluster assembled materials.

The present work was conducted along both an experimental and a theoretical line. Experimentally, relative thermodynamic stabilities together with ionization potentials are presented for selected cluster sizes. To assist in rationalizing some of the experimental findings, in particular those outside the scope of a jellium model, we carried out quasi-relativistic

[a)]Permanent address: Nestlé Research Center, Department of Food Technology, CH-1000 Lausanne 26, Switzerland.

 0021-9606/96/105(13)/5574/12/$10.00

density functional calculations continuing our previous quantum chemical studies on mixed metal clusters.[19] Some structural information was obtained by a symmetry constraint geometry search on a series of selected clusters. The resulting structural models are in good agreement with experimental observations. Moreover, atomization and fragmentation energies as well as first ionization potentials, electron densities, and dipole moments have been calculated in order to achieve an overall characterization of the cluster electronic structure.

II. EXPERIMENT

The experimental methods used for this research include (i) cluster generation by supersonic expansion of a mixed metal vapor from a high-temperature two-chamber oven under well characterized thermodynamic conditions, (ii) photoionization and electron impact mass spectroscopy at fixed photon and electron energies to obtain the relative thermodynamical stabilities of the generated clusters, and (iii) measurements of photoionization efficiency (PIE) curves from which vertical ionization potentials are extracted.

A. Experimental setup

The experimental setup has been previously described and only cursory details are given here.[20–22] The mixed metal clusters have been studied in a molecular beam apparatus which consists of a source chamber and an analysis chamber. The two chambers are separated by a 1 mm skimmer and were pumped differentially to pressures of 3×10^{-6} and 5×10^{-7} Torr, respectively. For mass spectral analysis the neutral cluster beam was ionized within the ion extraction region of an Extrel C50 quadrupole mass spectrometer (upper mass limit of 4000 amu). The ionizing light source was the output of a 1 kW Xe arc lamp (unstructured emission spectrum below 380 nm) which was dispersed through a 0.25 m monochromator (PTI; 1200 lines/mm, grating blazed at 300 nm). The spectral resolution was set either to 16.6 nm full width at half maximum (FWHM) to measure mass spectra, or 6.6 nm for obtaining the photoionization efficiency curves. For subsequent normalization, the photon flux was measured with a calibrated EMI 9783 B photomultiplier. For electron impact mass spectroscopy the electron energy was set to 27 eV. After mass separation the ion current was amplified with a dynode/channeltron combination and the signal was then transferred for further processing to a PDP 11/73 computer.

B. Cluster generation

In previous experiments on bimetal clusters both metals were added inside a single resistively heated reservoir (upper temperature limit 1250 K), precluding an independent control of the vapor pressures of the two metals.[23–25] In addition, the ratio of the vapor pressures varied during the experiment. These limitations have now been overcome by introducing a new two-chamber oven which consists of two separately heatable cartridges.[20] A first, large cartridge ($\sim$50 cm^3) used for the evaporation of the alkali metals can be resistively heated up to 1250 K. It is connected via a 25-mm-long, thin-walled tube (1 mm thickness) with a second, smaller gold containing cartridge ($\sim$15 cm^3) which can be radiatively heated to a maximum of 1800 K. The mixed metal vapor expands through a 30° conical/0.5-mm-diam nozzle into the vacuum where cluster growth occurs under conditions of high supersaturation via homogeneous nucleation. With proper choices of materials and insulations, a difference in temperature of 1000 K can be maintained during the measurements.

For the Na/Au coexpansion the large cartridge was filled with 20 g of sodium and heated to 1100 K ($p_{Na}\approx$450 Torr). The high-temperature cartridge was loaded with 6 g of gold and heated to 1800 K ($p_{Au}\approx$0.05 Torr). Once the final temperatures of both cartridges were reached, stable experimental conditions could be maintained for about 80 min.

The Cs_xAu clusters were generated in a different way. The difficulties normally encountered when handling pure cesium metal were circumvented by synthesizing metallic cesium *in situ* from calcium and cesium chloride by the following reaction:

$$\tfrac{1}{2}\,\mathrm{Ca}(c)+\mathrm{CsCl}(c)\xrightarrow{900\ \mathrm{K}}\tfrac{1}{2}\,\mathrm{CaCl_2}(c)+\mathrm{Cs}(g)$$

$$\Delta G^{\circ}_{900}\cong 9[\mathrm{kJ\ mol^{-1}}].$$

The equilibrium constant thus predicts about 220 Torr Cs vapor pressure at 900 K. The cartridge was filled with 95 g of CsCl and 17 g of Ca (Cs/Ca mol fraction of 1.3) and the salt was carefully mixed with the metal. This was done inside a dry box to prevent the vacuum packed calcium metal from incurring an oxide layer. The cartridge was then transferred into the oven and heated to approximately 900 K (220 Torr). As for the Na/Au expansions, the small cartridge was filled with 6 g of gold and heated to 1800 K. Once the final temperatures of both cartridges were reached, about 50 min of stable beam conditions were available for experimentation. Besides mixed Cs_xAu_y clusters, chlorine containing species were also generated in the expansion. These will not be discussed here.

C. From mass spectral abundances to cluster stabilities

To connect mass spectral ion abundances with thermodynamic stabilities of the neutral clusters, several experimental questions have to be addressed.[26–28] *First*, one has to make sure that the neutral size distribution reliably reflects differences in thermodynamic stability. Extensive studies have previously been performed to assess the impact of the source temperature and nozzle geometry on cluster-size distributions and cluster temperatures.[20,21] In the experiments reported here, the source conditions were chosen such that the neutral size distributions reflect, as close as possible, relative thermodynamic stabilities. *Second*, for mass spectral detection, clusters have to be ionized, rendering the measured ion current a function of the ionization cross section of the corresponding cluster. A procedure was developed[20,23] which, provided the PIE curves are known, allows for the

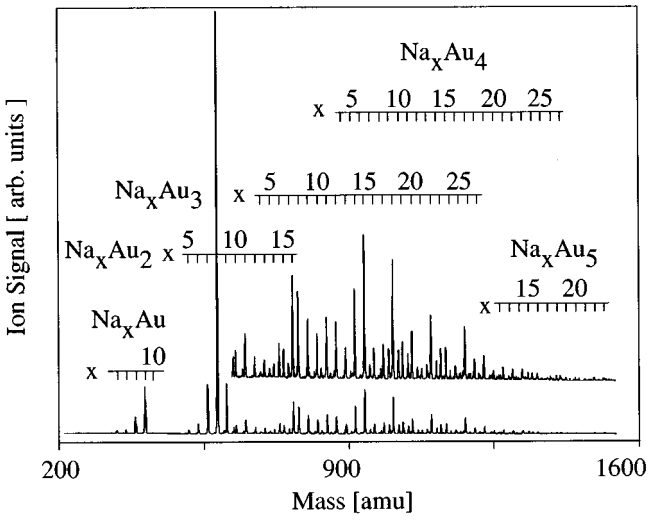

FIG. 1. Representative photoionization mass spectra of mixed Na_xAu_y clusters. The clusters are generated in a two-chamber oven. The mixing ratio of the two metal vapors is controlled via the temperatures of the chambers, one containing alkali and the other gold metal. The temperature of the large chamber containing sodium is 1100 K. The small gold chamber is kept at 1800 K, corresponding to a vapor pressure of 0.05 Torr. The clusters are ionized with a 1 kW Xe arc lamp (unstructured emission spectrum below 380 nm), dispersed through a 0.25 m monochromator (PTI; 1200 lines/mm, grating blazed at 300 nm). The Na_xAu_y clusters are ionized at 300 nm (16.5 FWHM).

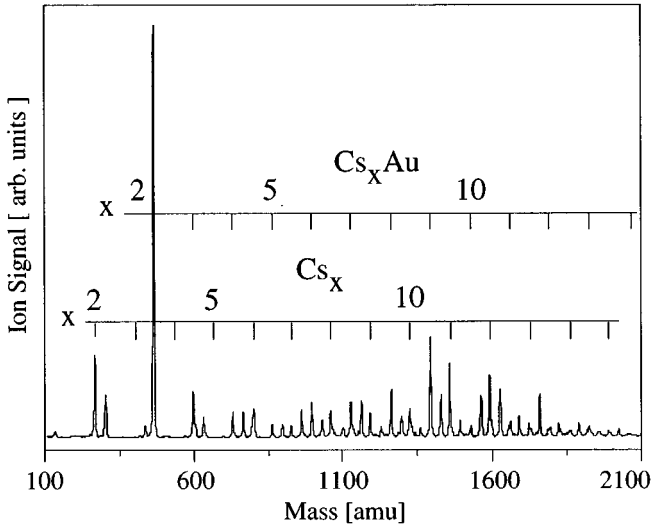

FIG. 2. Representative photoionization mass spectra of mixed Cs_xAu_y clusters. All procedures are as described in the caption to Fig. 1, except that the temperature of the Cs chamber is 900 K and that the Cs_xAu_y clusters are ionized at 350 nm (16.5 FWHM).

correction of the mass spectra for relative photoionization cross sections and at the same time reduces contamination from fragmentation.

D. From photoionization efficiency (PIE) curves to ionization potentials (IP)

Despite extensive theoretical and experimental evidence,[29–32] the connection between the PIE curve of a cluster and its vertical or adiabatic ionization potential (IP) is neither unique nor straightforward. The complications arise from the fact that ionization induced fragmentation, temperature, isomer distribution, and the electronic and vibrational spectra of the neutral as well as the ion are usually not known. Therefore, different assignment procedures have been proposed which are believed to yield internally consistent relative vertical IPs.[32–35] Here, we apply the assignment procedure termed *pseudo-Watanabe* which in the past has proven to be rather robust and reliable.[32]

III. RESULTS

Figure 1 shows a photoionization mass spectrum from a mixed sodium/gold expansion. It is dominated by the presence of Na_8Au_2. Heteroclusters with up to five gold atoms are observed. The mono- and digold heteroclusters show a strong multimodal distribution. Such a clear size dependence of cluster intensities is not observed for heteroclusters with three or more gold atoms. On the other hand, the mass spectrum of a cesium/gold expansion at similar vapor pressures (Fig. 2) reveals a strong Cs_2Au mass peak and only heteroclusters with one cesium atom are detected. Another distinction in these expansions is the production of pure cesium clusters. The observed chloride clusters (Cs_xCl, Cs_xAuCl) which appear as additional peaks will not be discussed in this work.

As shown in the experimental section, measured mass spectral intensities have to be corrected for relative photoionization cross sections before conclusions regarding relative stabilities of the neutral species can be drawn.[20,23] The corrected intensity distributions of Na_xAu and Cs_xAu are shown as stick spectra in Figs. 3 and 4, respectively. These are believed to reliably reflect relative thermodynamic stabilities of the neutrals. The multimodal distribution of neutral Na_xAu stabilities (Fig. 3) shows a first relative maximum at Na_3Au and a second absolute one at Na_9Au which are both

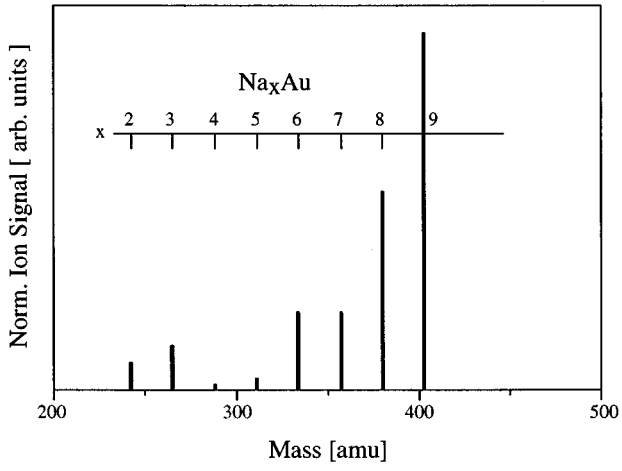

FIG. 3. Corrected intensity distributions of mixed Na_xAu clusters. These spectra reflect as close as possible the neutral cluster distributions prior to ionization (see Ref. 23).

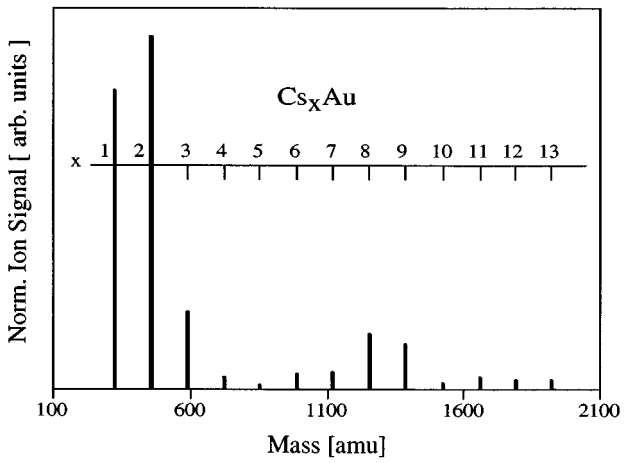

FIG. 4. Corrected intensity distributions of mixed Cs_xAu clusters. These spectra reflect as close as possible the neutral cluster distributions prior to ionization (see Ref. 23).

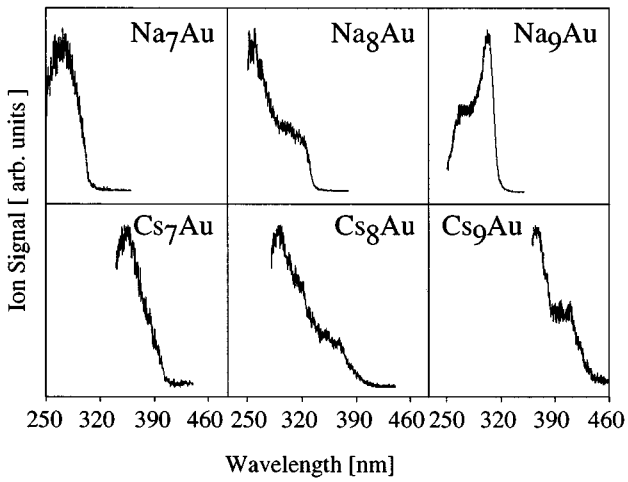

FIG. 5. Intensity-normalized photoionization efficiency curves for Na_xAu and Cs_xAu, $x=7,8,9$. Details concerning measurement and assignment of ionization potentials are given in the text. The spectra are obtained at a monochromator resolution of 6.6 nm. The vertical ionization potentials, given in Fig. 6 and Table I, are extracted from the near-threshold regions within 0.5 eV of the ionization onset using pseudo-Watanabe plots (see Ref. 32).

followed by flat areas of low intensity. Essentially no Na_xAu clusters are formed beyond Na_9Au. In contrast, the multimodal Cs_xAu distribution (Fig. 4) is dominated by CsAu and Cs_2Au which are the two smallest clusters with Cs_xAu clusters extending up to about $Cs_{13}Au$. Strong drops in intensity are found after Cs_3Au and Cs_9Au—analogous to Na_xAu—yet with maxima shifted down by one alkali atom, at Cs_2Au and Cs_8Au. The appearance of CsAu in Fig. 4 deserves particular attention. This species is not present in the photoionization mass spectrum (Fig. 2). The reason for this is its low ionization cross section at 350 nm. Its relative stability is estimated from a cluster distribution ionized by impact with a 27 eV electron beam.[20]

Photoionization efficiency curves are measured for the most stable clusters. They are shown for Na_xAu and Cs_xAu ($x=7$–9) in Fig. 5. Using a procedure described in Ref. 32, the ionization potentials are determined from the low-energy onsets of the PIE curves. These are tabulated in Table I and shown graphically in Fig. 6. For comparison, published ionization potentials of Na_x are also included in Table I and Fig. 6.[32]

The most important experimental results can be summarized as follows:

(i) Neutral monogold heteroclusters of sodium and cesium show strong stability maxima at Na_9Au and Cs_2Au, respectively. In cesium/gold expansions, Cs_8Au is the most stable cluster in the higher mass range, but its dominance is much less pronounced. At variance with this experimental finding, Cs_9Au is calculated to be the most stable cluster in the high mass range (see Sec. B).

(ii) The ionization potentials of the sodium–gold heteroclusters Na_xAu ($x=7$–9) are similar to those of isoelectronic pure sodium clusters, with the known odd–even effect and a drop of the ionization potential when going from the octamer ($x=7$) to the nonamer. In contrast, for Cs_xAu ($x=7$–9) this odd–even effect is reversed, showing a larger ionization potential for Cs_8Au than for Cs_7Au. In this mass range the ionization potentials of the cesium–gold heteroclusters are up to 1 eV smaller than the ones of the corresponding sodium–gold heteroclusters due to the lower binding energy of the cesium atom valence electron.

(iii) With cluster intensities of one order of magnitude larger and heteroclusters with up to five gold atoms, the gold and sodium have a substantially higher tendency towards heterometal bond formation and aggregation than their cesium/gold counterparts. This behavior mimics the trend in the corresponding bulk heat of formation values.[10]

IV. DISCUSSION

Our primary motivation for this work is to elucidate electronic and structural properties of mixed metal clusters and to correlate trends and features at the nanoscopic limit with bulk properties. The $(alkali)_xAu$ clusters are here a par-

TABLE I. Ionization potentials (IPs) of $Na_{x-1}Au$ and $Cs_{x-1}Au$ clusters (in eV). For comparison, we also include the IPs of pure sodium clusters Na_x from Ref. 32 which have been measured and analyzed by the same method as used in this work.

x	Na_x	$Na_{x-1}Au$	$Cs_{x-1}Au$
3	3.90	⋯	3.24
4	4.24	⋯	3.40
5	3.99	⋯	⋯
6	4.23	⋯	⋯
7	4.03	4.01	⋯
8	4.22	4.13	3.09
9	3.56	3.75	3.16
10	3.84	3.97	2.91

ticularly attractive system. One is able, on the one hand, to relate our findings to a large body of experimental and theoretical work on pure and mixed monovalent clusters.[20,36–38] On the other hand, the properties and trends of alkali/gold intermetallic compounds can hopefully provide clues for an interpretation of the Na_xAu and Cs_xAu cluster data.[8]

In a first part (Sec. A) the experimental results are discussed within the framework of a spherical shell model. In a second part (Sec. B) extensive quantum chemical calculations with inclusion of relativistic effects provide a solid basis for the interpretation of the experimental results. Finally, in Sec. C, we compare the properties of the mixed-metal clusters to those of the corresponding alkali–gold intermetallic compounds.

A. Electronic shell model

A widely used approach in the interpretation of monovalent metal cluster data is the jellium model.[36,39–41] Experimentally, the electronic shell structure can be demonstrated in several ways. An often discussed probe is the measurement of mass spectral intensity distributions where maxima are expected at shell closings. A more direct probe is the determination of ionization potentials. Both these approaches have been used here.

1. Mass spectral intensity distributions

The corrected mass spectrum of Na_xAu (Fig. 3) shows a pronounced maximum followed by a ledge at Na_9Au (10 valence electrons). Ten-electron maxima have already been observed in the past and interpreted via a modified level order relative to pure alkali clusters.[24,40,42] Assuming the single gold atom is sitting at the center of the cluster, its higher ionization potential causes a depression of the potential well at the center. This leads to a selective stabilization of ns states and eventually to a reversal of the $1d/2s$ levels (level order: $1s,1p,2s$). The mass spectral distribution of the Cs_xAu clusters shows a ledge at Cs_9Au as well (less pronounced than for Na_xAu). However, the relative intensity maximum occurs for Cs_8Au.

2. Ionization potentials

One straightforward observable of the shell structure is the ionization potential and its trend as a function of cluster size.[41,43,44] An odd–even alternation is predicted, clusters with an odd number of electrons having a smaller IP than those with an even number. Up until now all IP measurements on pure or mixed monovalent clusters conform to this prediction, including the values for Na_xAu reported here (Fig. 6). Turning our attention to the Cs/Au system, we see that this trend is reversed in the range Cs_xAu, $x=7–9$. The IP of Cs_8Au is larger than those of Cs_7Au and Cs_9Au.

A shell model in which all s valence electrons contribute to the sea of delocalized electrons seems appropriate to describe Na_xAu mixed clusters. On the other hand, the reversed odd–even alteration in the ionization potentials of the Cs_xAu clusters cannot be understood within a simple electronic shell model. An alternative electronic shell description was

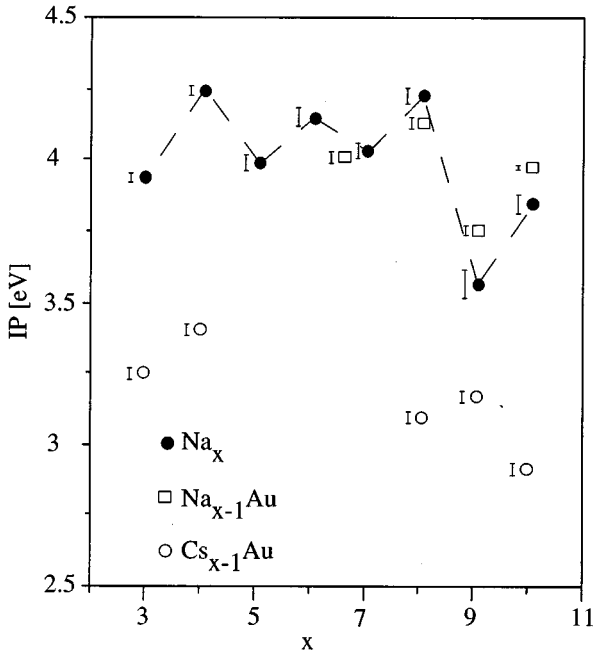

FIG. 6. Ionization potentials of $Na_{x-1}Au$ and $Cs_{x-1}Au$ plotted against the total number of atoms x (equal to the number of valence electrons). For comparison we also include the ionization potentials of Na_x from Ref. 32, measured and analyzed according to the same procedure.

applied in the past to explain results for compound clusters such as Cs_xO_y,[42] Na_xO_2,[45] and Na_xCl.[46] Stabilities and ionization potentials are nicely interpreted, assuming that each oxygen (chloride) consumes two (one) electrons from the sea of delocalized electrons of the alkali clusters. Referring to the large difference in electron affinity between Cs and Au,[13] we may similarly assume that the gold atom takes up one valence electron from the cesium cluster to form a filled s-orbital (an ''inert'' pair!), $[Xe]4f^{14}5d^{10}6s^2$. The Cs_xAu cluster is then more appropriately described as $Cs_x^+Au^-$ or $Cs_{x-1}(CsAu)$ and stabilities are derived from the shell structure of Cs_x^+ or Cs_{x-1}. The very intense peaks for CsAu and Cs_2Au are indeed suggestive of the existence of a stable CsAu or CsAuCs block inside Cs_xAu clusters, i.e., a Cs-solvated CsAu heterodimer or CsAuCs trimer (analogous to known dialkali monohalides).[47] Similar arguments might also be invoked for Na_xAu clusters, since the difference in electron affinity is again substantial.[13] The ledges in the mass spectra at Na_3Au, Na_9Au and Cs_9Au would thus correspond to 2 and 8 e closed shell alkali clusters.

Based on the experimental database presented here, it is not possible to choose definitively between a pure jelliumlike model or one containing partial ionic interactions. However, the following theoretical description indicates that the inert pair model is well suited only for Cs_xAu clusters, while for the Na_xAu series all s valence electrons contribute to the jellium electron ''reservoir.'' With this difference in mind, one may characterize the cluster bonding of Na_xAu as mainly polar covalent and that of Cs_xAu as more ionic.

B. Quantum chemical investigations

1. Model aspects and computational details

It is well known that the electronic structure of gold compounds exhibits significant relativistic effects.[48] Therefore, the present alkali gold clusters require a quantum chemical method which allows the inclusion of such relativistic effects. We have chosen the scalar relativistic variant[49] of the ''first principles'' linear combination of Gaussian-type orbitals density functional (LCGTO-DF) method[50] which has been shown to provide an efficient, yet accurate approach to the electronic structure of gold compounds.[51,52] We performed all-electron self-consistent field (SCF) calculations using the local density approximation (LDA) to the exchange-correlation energy functional as suggested by Vosko, Wilk, and Nusair (VWN).[53] After self-consistency had been reached, the total energy was evaluated for the resulting electron density employing gradient corrections to the exchange[54] and to the correlation[55,56] energy functionals according to the generalized gradient approximation (GGA). This approximate procedure for taking into account ''nonlocal'' corrections to the exchange-correlation energy is quite economical, yet often of sufficient accuracy.[57]

The orbital basis set for Au, $(21s,17p,11d,7f)$ contracted to $[11s,10p,7d,3f]$, was taken as in our previous work.[58] A basis set of the type $(12s,8p,1d)\rightarrow[6s,5p,1d]$ (d exponent: 0.122) was used for Na[59] and a $(23s18p12d)\rightarrow[13s11p6d]$ basis set for Cs.[60] All orbital basis sets were contracted in a generalized fashion using relativistic LDA atomic eigenvectors. The accuracy of the basis sets may be judged by the rather small basis set superposition error (BSSE) for the calculated dimer binding energy of NaAu and CsAu (about 0.01 eV). In the LCGTO-DF method two auxiliary basis sets were used to fit the electron density and the exchange-correlation potential. These fitting basis sets were constructed in a standard fashion[49] from the exponents of the various orbital basis sets.

The cluster geometries were optimized at the relativistic gradient corrected level of the theory. Since no analytic gradients of the total energy were available for the relativistic variant of the LCGTO-DF method, the energy minimization had to be carried out employing a cyclic strategy involving each degree of freedom under an imposed symmetry constraint. The search was stopped when all interatomic distances were altered by less than 0.005 Å. Once the equilibrium geometry had been determined, the cluster binding energy was analyzed by calculating the cluster fragmentation energy, i.e., the energy required to formally abstract the gold atom from the otherwise unchanged alkali moiety, as well as atomization energies of the whole cluster and of the alkali moiety. Ionization potentials were obtained at the ΔSCF level as differences of the corresponding total energies.

In the present investigations we considered the Na_7Au, and Cs_7Au clusters in both D_{5h} and C_{6v} symmetry, Na_8Au and Cs_8Au in D_{4d} symmetry, and Na_9Au and Cs_9Au in D_{3h} symmetry (see Fig. 7). The symmetry constraints were chosen based on the results of a previous, more elaborate theoretical comparison[19] between Na_6Mg and Na_6Pb clusters, which indicated that the heavy hetero-atom (differently from light magnesium) preferentially occupies the central position of the cluster. Therefore, to reduce the computational effort, we restricted our calculations to geometries which feature a high coordination of alkali atoms around gold, with one exception to be discussed below in more detail. Comparing the results for the clusters M_7Au, M=Na, Cs, in D_{5h} and C_{6v} symmetry (Tables II and III) we note that the binding energy is noticeably higher for the case where gold is higher coordinated. The latter symmetry has been included to allow a more direct analysis of the charge distribution in the clusters as the other symmetries prevent the formation of a nonzero dipole moment (see below). However, the geometric structure of all the alkali gold clusters investigated is not expected to be rigid, but rather fluxonial, characterized by potential energy surfaces with several shallow minima of comparable depth. The methodology employed here would have rendered a global search of such a surface rather expensive, if not impossible. On the other hand, the electronic structure is not expected to significantly change for moderate geometry alterations, as suggested by the more detailed comparison carried out for the mixed-metal cluster Na_6Pb.[19] Under these circumstances, a constraint symmetry optimization seems to provide an acceptable compromise between accuracy and computational expense.

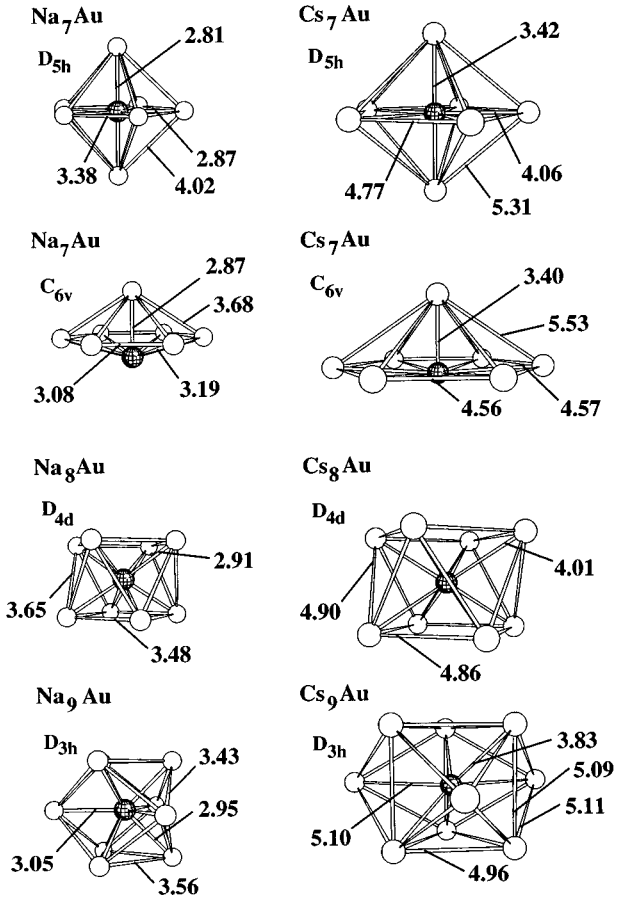

FIG. 7. Optimized geometries of Na_xAu and Cs_xAu clusters from density functional calculations employing a gradient-corrected exchange-correlation functional (see text). Bond lengths are in Å.

TABLE II. Calculated atomization energies ΔE_{at} and fragmentation energies ΔE_{fr} for various processes are shown together with calculated and experimental ionization potentials (IP) and the highest occupied molecular orbital (HOMO)-lowest unoccupied molecular orbital (LUMO) gap $\Delta\epsilon$ for Na_xAu clusters ($x=7$–9) under various symmetry constraints. All energies are given in eV.

Cluster	Na_7Au		Na_8Au	Na_9Au
Symmetry	D_{5h}	C_{6v}	D_{4d}	D_{3h}
$\Delta E_{at}(Na_xAu \rightarrow xNa+Au)$	7.21	6.73	8.22	9.15
$\Delta E_{fr}(Na_xAu \rightarrow Na_x+Au)$	3.96	3.73	3.84	4.62
$\Delta E_{at}(Na_x \rightarrow xNa)$	3.25	3.00	4.38	4.53
$\Delta E_{at}(1/xNa_x \rightarrow Na)$	0.46	0.43	0.55	0.50
IP (calc.)	4.02	4.28	3.70	3.87
IP (exp.)[a]	4.13		3.75	3.97
$\Delta\epsilon$(HOMO-LUMO)	0.45	0.73	0.86(0.15[b])	0.84

[a]This work.
[b]Gap of majority spin manifold.

TABLE III. Calculated atomization energies ΔE_{at} and fragmentation energies ΔE_{fr} for various processes are shown together with calculated and experimental ionization potentials (IP) and the HOMO-LUMO gap $\Delta\epsilon$ for Cs_xAu clusters ($x=7$–9) under various symmetry constraints. All energies are given in eV.

Cluster	Cs-Au		Cs_8Au	Cs_9Au
Symmetry	D_{5h}	C_{6v}	D_{4d}	D_{3h}
$\Delta E_{at}(Cs_xAu \rightarrow xCs+Au)$	5.27	4.94	5.89	6.49
$\Delta E_{fr}(Cs_xAu \rightarrow Cs_x+Au)$	3.50	3.39	3.78	4.16
$\Delta E_{at}(Cs_x \rightarrow xCs)$	1.77	1.56	2.11	2.33
$\Delta E_{at}(1/xCs_x \rightarrow Cs)$	0.25	0.22	0.26	0.26
IP (calc.)	3.17	3.24	3.22	3.09
IP (exp.)[a]	3.09		3.16	2.91
$\Delta\epsilon$(HOMO-LUMO)	0.04	0.52	0.81(0.15[b])	0.65

[a]This work.
[b]Gap of majority spin manifold.

2. Optimized geometries

As can be seen from Fig. 7, the Na–Au bond lengths are rather constant in the series Na_xAu, $x=7$–9, while the Cs–Au bond lengths are spread over quite a wide range. The Na_xAu bond lengths vary from 2.81 to 3.19 Å (a range of 0.38 Å), whereas for Cs_xAu, they vary from 3.40 to 5.10 Å (a range of 1.70 Å). This finding indicates that in the Na_xAu clusters the Na–Au bonds are essentially equivalent, while in Cs_xAu large differences are present among the various Cs–Au bonds. This observation provides additional support for the hypothesis suggested by the experimental high abundance of CsAu and Cs_2Au in the molecular beam that specific CsAu subunits are present in the larger Cs_xAu clusters. A direct comparison of the Na_9Au and Cs_9Au clusters is also informative. While the former shows the usual close similarity between the two different Na–Au bonds (2.95, 3.05 Å), the latter exhibits two types of coordination spheres. The first shell, with a closer Cs–Au distance of 3.83 Å, is formed by the six ''quasi-axial'' cesium atoms. The three ''equatorial'' Cs atoms capping the three rectangular faces of the trigonal prism of the first Cs shell are rather far from the central gold atom (5.10 Å); these Cs atoms are forming a second shell (Fig. 7). With only one coordination sphere in the Na_xAu clusters, but more than one in the Cs_xAu clusters, one is able to explain the distinct ledge following Na_9Au in the experimental abundance spectrum and the rather dispersed abundances following Cs_9Au. The calculated Na–Na and Cs–Cs bond lengths are somewhat shorter or almost equivalent to the sum of the covalent radii of the corresponding atoms.[61] This suggests that the bonding interaction among the alkali metal atoms might provide an important contribution to the overall cluster stability, as will be discussed in detail in the next subsection.

3. Calculated stabilities

As can be seen from Table II, the atomization energies of the series Na_xAu, $x=7$–9, increases by about 1 eV for each additional sodium atom in the cluster. This result agrees well with the clearly increasing stability as deduced from the experimentally obtained relative abundances (Fig. 3). The atomization energy of the mixed-metal clusters may be separated into two contributions: the fragmentation energy, i.e., the energy required to separate the gold atom from the alkali fragment, and the atomization energy of the remaining alkali metal fragment itself. In these formal separation processes the geometry of the alkali fragments is kept optimized for the mixed-metal cluster. For all sodium clusters investigated, these two contributions are nearly equal, 3.7–4.6 eV for the fragmentation energy and 3.0–4.5 eV for the atomization of the alkali fragments. For all Na moieties an average contribution of about 0.5 eV per sodium atom to the alkali fragment stability has been calculated (Table II). At this point it is worth nothing that the stability increase of Na_8Au compared to Na_7Au, both in D_{5h} and C_{6v} symmetry, is essentially due to increased Na–Na interactions, while the stability gain of Na_9Au compared to Na_8Au arises mainly from the Na–Au interaction. This finding may be interpreted as follows: when a sodium atom is added to Na_7Au to form Na_8Au, the coordination sphere around the gold atom is filled and optimal Na–Na interactions result. The subsequent buildup step to Na_9Au is less favored by Na–Na interactions, since the attractive interaction within the Na moiety is essentially compensated for by the concomitantly increasing steric repulsion. Thus the overall binding energy increase in Na_9Au is due to markedly stronger Na–Au interactions.

A similar analysis for cesium clusters (Table III) leads to a different interpretation of the cluster stability. First, the atomization energy of the mixed-metal clusters increases along the series by only 0.6 eV per additional cesium atom. The average atomic contribution to the stability of the Cs moieties is only about 0.25 eV (Table III). As a consequence, the cluster fragmentation energy and the atomization contribution of the alkali moiety no longer contribute equally to the cluster stability. The cesium–gold fragmentation energy amounts to about two thirds of the cluster stability, while only one third is ascribed to the Cs–Cs interaction. Thus, in the Na_xAu series each Na atom is almost equally strongly bonded to Au and to the other Na atoms, while in Cs_xAu each Cs is mainly bonded to the gold atom, the Cs–Cs inter-

TABLE IV. Fragmentation energies of M_7Au (M=Na, Cs; both for D_{5h} and C_{6v}) for a separation of the clusters into the subunits and the corresponding number of alkali atoms M as well as atomization energies of the fragments MAu and M_2Au. All energies are given in eV.

	M			M	
D_{5h}	Na	Cs	C_{6v}	Na	Cs
$M_7Au \rightarrow M_2Au + 5\ M$	4.07	2.06	$M_7Au \rightarrow MAu + 6\ M$	4.33	2.29
$M_2Au \rightarrow Au + 2\ M$	3.14	3.21	$MAu \rightarrow Au + M$	2.40	2.65
$M_7Au \rightarrow Au + 7\ M$	7.21	5.27	$M_7Au \rightarrow Au + 7\ M$	6.73	4.94

actions being much less important. It seems worthwhile to elaborate this last statement by exploring the influence of smaller alkali–gold clusters as substructures, (M=Na,Cs), possibly also as intermediates on the way to a total cluster fragmentation. To this end, the fragmentation energies of the alkali–gold clusters into subunits MAu and M_2Au and in the remaining free alkali atoms have been calculated, together with the atomization energies of the subunits for both Na_7Au and Cs_7Au in C_{6v} and D_{5h} symmetries (Table IV). Obviously, the atomization energies of the subunits MAu and M_2Au are very similar for sodium and cesium (they differ at most by 0.25 eV), while the fragmentation energies of the starting clusters differ much more (by more than 2.0 eV) and are lower for the cesium clusters. This finding implies that the contribution to the total cluster atomization energy derived from the subunit is larger for cesium clusters and may be taken as a quantitative indication for the existence of these subunits.

The experiments seem to indicate that Cs_8Au is the most stable cluster in the Cs_xAu series, a result which is at variance with the present calculations. It is not easy to explain this apparent discrepancy between theory and experiment. However, considering that the difference in mass spectral intensity between Cs_8Au and Cs_9Au is rather small, it is quite conceivable that the measured relative abundances do not reflect the actual thermodynamic stabilities with the required accuracy. The fragmentation of the clusters into smaller subunits could be the principal cause for the deviation from equilibrium. As has already been pointed out above, sodium atoms are much more strongly bonded to each other in Na_xAu clusters than the cesium atoms in Cs_xAu. This suggests that in the Na_xAu series rather strong Na–Na bonds must be broken in a hypothetical transition state of the fragmentation process. On the other hand, since Cs–Cs bonds are significantly weaker in Cs_xAu, one expects a lower activation energy for the fragmentation which in turn would make it substantially more difficult to reach experimental conditions that correspond to thermodynamic stability.

4. Calculated ionization potentials

The theoretical ionization potentials of Na_xAu clusters are in good agreement with the measurements (Table II), deviating at most by 0.1 eV. The calculated and measured ionization potentials exhibit the same odd–even effect. For Cs_xAu the reversed odd–even effect observed in the experiments is nicely paralleled by the theoretical results (maximum difference between theory and experiment: 0.2 eV), although the oscillation amplitude is much reduced compared to Na_xAu. The trends of the ionization potentials may profitably be discussed with the help of an orbital correlation diagram based on the Kohn–Sham levels. In fact, these one-electron energies may be interpreted as orbital electro negativities via the Slater–Janak theorem[62,63] which also provides a relationship to ionization potentials by invoking Slater's ''transition state'' concept.[62] In the present case we expect the ground state Kohn–Sham spectrum to give a reliable description of the relevant valence shell ionization potentials because the orbitals under study are highly delocalized and therefore a transition state procedure implies a more or less uniform ''relaxation'' shift to lower orbital energies, keeping the level ordering essentially unchanged.

As an example, the orbital correlation diagrams of Na_9Au and Cs_9Au are constructed with respect to their fragments in Fig. 8. (The subsequent conclusions have been verified also for the other clusters of the present investigation.) The levels can be classified according to the jellium model as (Au $5d^{10}$) $1s^2 1p^6 2s^{x-7}$ for Na_xAu and as (Au $5d^{10}6s^2$) $1s^2 1p^{x-3}$ for Cs_xAu. Of course the assignment of the Au 6*s* derived orbital, which is in one case (Na) counted as a jel-

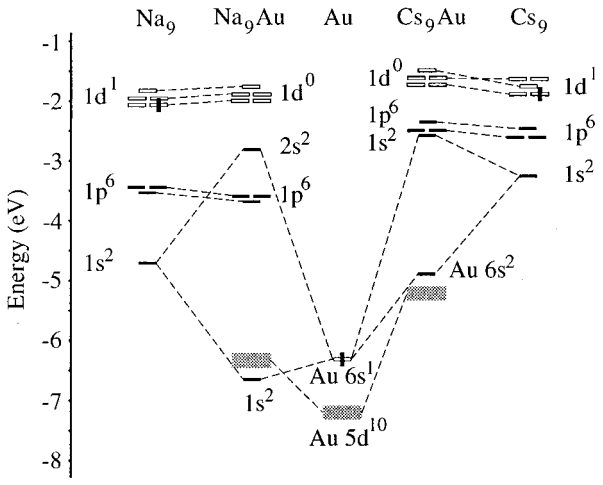

FIG. 8. Orbital correlation diagram based on Kohn–Sham energies for the assembly of the Na_9Au and Cs_9Au (D_{3h}) clusters from their fragments Au, Na_9 and Cs_9 (D_{3h}). Where meaningful, the levels are labeled according to the jellium model; the manifold of Au 5*d* orbitals is represented by shadowed gray boxes. Filled and open levels indicate doubly occupied and empty orbitals, respectively; for open shells the unpaired electron is explicitly given as a vertical bar.

TABLE V. Shifts $\Delta\epsilon$ of Kohn–Sham core level eigenvalues[a] for Na_7Au (C_{6v}) and Cs_7Au (C_{6v}) clusters as well as for the corresponding Na_7 (C_{6v}) moieties. For the alkali atoms, axial and equatorial positions are discriminated. All energies are in eV.

		Na $2p$		Cs $4d$		Cs $4p$	
Core level	Au $4f$	Ax.	Eq.	Ax.	Eq.	Ax.	Eq.
Na_7Au	+0.93	+0.63	+0.49				
Na_7		+0.90	+0.35				
Cs_7Au	+1.96			+0.45	+0.43	+0.45	+0.43
Cs_7				+0.57	+0.32	+0.57	+0.32

[a]Shifts calculated with respect to Kohn–Sham eigenvalues of free atoms: ϵ(Au $4f$) $=-81.01$ eV, ϵ(Na $2p$) $=-28.71$ eV, ϵ(Cs $4d$) $=-74.17$ eV, ϵ(Cs $4p$) $=-160.46$ eV.

lium 1*s* level and in the other case not (Cs), is a simplification that relies on the dominant character of this molecular orbital. Already here we see a principal difference in the Na–Au bonding of the clusters Na_xAu and Cs_xAu. In the first systems, the bonds are of polar covalent-type (with a jellium of $x+1$ electrons), while in the second they may be described as ionic, $(Au^-)-(Cs_x^+)$, where a jellium of $x-1$ electrons is assigned to the Cs_x moiety.

The most important finding of the level analysis is that for Na_xAu the jellium shell structure is evident (the levels 1*p* and 2*s* are separated by about 0.8 eV in Na_9Au), rationalizing the maxima for the ionization potentials of the closed-shell clusters Na_7Au and Na_9Au. On the other hand, in Cs_xAu the levels 1*s* and 1*p* are almost degenerate, in line with the weaker Cs–Cs interaction. The lower oscillation amplitude of the ionization potentials in the cluster series Cs_xAu is in line with this observation. On the other hand, the unexpected trend in the series $x=7$–9, namely a larger measured and calculated ionization potential for the odd-electron system with $x=8$ than for the even-electron systems $x=7,9$, clearly shows that a simple rationalization on the basis of jellium-type shells does not apply in the case of Cs_xAu. It is interesting to note also that the one-electron energies of the highest occupied molecular orbital (HOMO) display the same trend as the ionization potentials. However, this last finding may be fortuitous because of the rather small differences in the one-electron energies ($\sim$0.05 eV) and since it may to some extent depend on the assumed symmetry constraints.

As a final observation from Fig. 8, it is worth noting the different energy shifts of the Au 5*d* orbitals: these levels are destabilized with respect to the free Au atom, but the destabilization in Cs_9Au is 1.1 eV stronger than in Na_9Au. This observation suggests that the gold atom carries a more negative charge in Cs_9Au than in Na_9Au and this is corroborated by the very similar shift (1.2 eV) displayed by the Au $4f$ core level. The same behavior has been observed for both the Na_xAu and Cs_x Au series, with differences in the Au 5*d* core level energies ranging from 0.9 to 1.2 eV thus paralleling those of the Au $4f$ core level.

5. Comparison of Na_7Au and Cs_7Au in C_{6v} symmetry

In order to gain a better understanding of the main differences in the electronic structure of the two cluster series Na_xAu and Cs_xAu, two representative clusters will be compared in more detail. Na_7Au and Cs_7Au in C_{6v} symmetry have been selected because they are the only model clusters which exhibit a nonzero dipole moment (pointing along their sixfold symmetry axis). Therefore additional information on the electron charge distribution in the clusters may be gleaned from this observable.

Both the total electron density as well as the differential density, i.e., the difference of the cluster electron density and the superimposed fragment electron densities (atomic gold and the alkali metal moiety), are displayed in Fig. 9. The following differences in the total electron density (upper panels) are observed. While in Na_7Au the density is uniformly distributed among the bonds, in Cs_7Au the density is noticeably greater along the Cs–Au axial bond than along the Cs–Au equatorial bonds. This is in good accordance with previous conclusions derived from the optimized geometrical structures, which lead us to classify the Na–Au bonds as

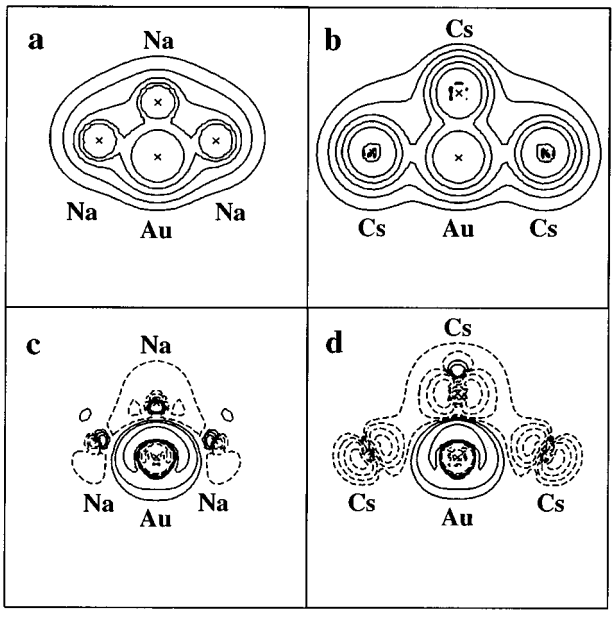

FIG. 9. Total (upper panels) and differential (lower panels) electron density plots for the Na_7Au and Cs_7Au clusters, calculated with a C_{6v} symmetry constraint. The plots display a plane which contains the sixfold axis and two of the six equivalent alkali metal atoms as well as the gold atom. The values of the contour lines are $10^{-n/2}$, $n=3(1)7$ a.u.; solid and dashed lines represent positive and negative values, respectively.

more or less uniform in the cluster but which pointed to the existence of Cs–Au subunits in the larger clusters. The latter hypothesis is also suggested by the experimental data. The differential density plot for $[\rho(Na_7Au)-\rho(Au)-\rho(Na_7)]$ [Fig. 9(c)] shows that a rather complex charge redistribution occurs in Na_7Au, whereby the electron density increases on the gold atom and is depleted on the Na_7 fragment moiety. This charge rearrangement is accompanied by significant polarization effects both on the gold and on the equatorial Na atoms. This leads to a local induced dipolar contribution whose vectorial sum points from the axial Na to Au, i.e., the gold atom represents the positive end of the dipole. It is worth noting that these induced dipoles are oriented opposite to the dipole caused by the Na–Au charge separation along the main symmetry axis which points from Au to the axial Na atom. The differential density plot of $[\rho(Cs_7Au)-\rho(Au)-\rho(Cs_7)]$ is much simpler: there is a definite and uniform charge transfer from the Cs_7 fragment as a whole to the gold atom, and no induced dipoles seem to be present at all. This differential density analysis corroborates the previous classification that while in Na_7Au the Na–Au bonds may be termed ''polar covalent'', in Cs_7Au the Cs–Au binding is of ionic character accompanied by an actual charge transfer between the two types of hetero atoms.

To quantify the charge separation we have calculated the dependence of the dipole moment of these two clusters for different positions of the gold atom along the symmetry axis, keeping the geometry of the alkali metal moiety fixed in the equilibrium structure (Fig. 10). If a linear variation of the dipole moment is observed in such an analysis, charges may be assigned based on the dynamic dipole moment, i.e., on the displacement derivative of the dipole moment, by assuming a simple model of rigid point charges. In the case of Na_7Au a rather linear variation of the dipole moment is found indeed. The corresponding charge separation is 0.50 a.u. with gold being negatively charged. This is in good agreement with all previous considerations concerning the cluster charge distribution. However, it should be mentioned that at the equilibrium geometry the small dipole moment (0.24 a.u.) points *toward* the gold atom, i.e., the gold atom represents the positive end of the dipole. This apparently strange behavior may be understood by considering the local dipole moments carried by the equatorial Na atoms which are clearly visible in the differential density plot (Fig. 9). In Cs_7Au the variation of the dipole moment is not linear at all, but almost constant in the vicinity of the equilibrium structure. This may be explained by assuming that the highly polarizable jelliumlike valence electrons of the equatorial Cs_6 moiety are apparently able to screen the geometrically induced change of the cluster dipole moment which is mainly due to the Au^-Cs^+ subunit. However, for Cs_7Au the orientation of the dipole moment at the equilibrium geometry is in agreement with a negative charge on the gold atom.

In summary, the behavior of the dipole moment is quite surprising: in Na_7Au the dipole moment varies linearly with the displacement of Au, but nonlinearly in Cs_7Au. This suggests that the cluster polarization is higher in the latter case. However, at the equilibrium geometry of Na_7Au the dipole moment has the opposite sign as the charge separation indicated by the dynamic dipole moment. On the other hand, in Cs_7Au the sign of the dipole moment properly reflects the charge transfer implied by the change of the dipole moment. In order to understand this finding, it may be useful to introduce the following distinction concerning the polarization effects. In Na_7Au the polarization is deduced from the induced dipoles (visible in the differential density plot) which lead to the opposite sign of the total dipole moment at the equilibrium geometry: clearly a large polarization of the cluster electron distribution as a consequence of the *formation of the bond* between the alkali fragment and the gold atom. The linearity of the dipole moment curve suggests that the polarization remains rigid with respect to a *geometric distortion*. The opposite situation may be pictured for Cs_7Au: the ionicity of the Cs–Au bonds implies that during the bond formation the molecular orbitals are not so much *polarized*, but rather differently *populated* with respect to the fragments, as a consequence of the actual charge transfer. In this case, the electron charge distribution efficiently screens possible effects of a geometry distortion as can be deduced from the nonlinear behavior of the dipole moment: this implies that the shapes of the molecular orbitals change significantly with the geometry.

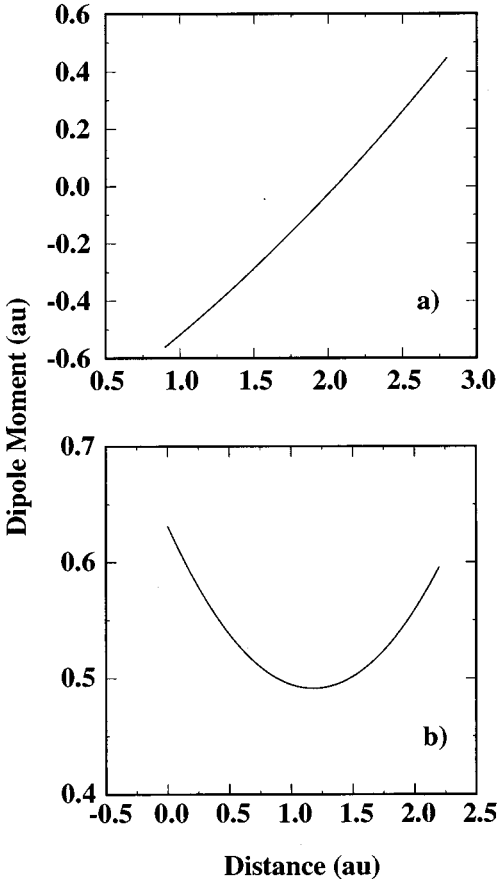

FIG. 10. Calculated dipole moment of Na_7Au (C_{6v}) (upper panel a) and of Cs_7Au (C_{6v}) (lower panel b) as a function of the distance of the gold atom from the base plane of the pyramid.

Finally, as a further assessment of the charge transfer inside these two clusters, we performed a core level analysis (Table V). In Na_7Au the Au $4f$ core level is destabilized by 0.9 eV with respect to the value in a free Au atom. The corresponding Au $4f$ core level shift in Cs_7Au is 1.9 eV. These shifts are consistent with a negative charge on the Au atom in the cluster, which is larger in Cs_7Au than in Na_7Au, in complete agreement with all previous considerations. The Na $2p$ core levels show a destabilization by 0.9 and 0.4 eV for axial and equatorial atoms, respectively, when going from the free atom to the Na_7 fragment. The (formal) insertion of a gold atom in Na_7Au leads to a stabilization of the $2p$ core levels of the axial Na atom by 0.3 eV, but to a further destabilization by 0.1 eV of the $2p$ levels of the equatorial Na atoms. These shifts may be ascribed to the electrostatic field inside the cluster: the core levels of the axial Na atom are stabilized because the Na_7 moiety is globally positive, while the core levels of the equatorial Na atoms feel the vicinity of the negatively charged gold atom and the two opposite effects partially cancel each other. For the Cs $4d$ and Cs $4p$ core levels, very small shifts are calculated, with the exception of a destabilization of 0.5 eV for both Cs $4d$ and Cs $4p$ in going from the free atom to Cs_7Au. This is apparently in contrast with the concept of a globally positive Cs_7 fragment, but it should be noted that while the positive charge is rather diffuse on the Cs_7 moiety (as can be verified in panel *d* of Fig. 9), the negative gold atom is much more compact and may be the actual cause of the calculated cesium core level destabilization.

C. Relations to NaAu and CsAu bulk compounds

At the end of the discussion we wish to come back to one of our initial motivations for this study—to connect concepts and properties at the nanoscopic molecular limit to the macroscopic bulk limit. The alkali/gold systems are an ideal testing ground for such explorations.[8,10]

1. Heat of formation

The tendency of gold for forming compounds is reported to increase from cesium to lithium.[7,9] This trend is confirmed by calculations.[10] At the cluster limit we observe that sodium and gold readily aggregate, forming mixed Na_xAu_y clusters over a large mass and compositional range. In contrast, mass spectral intensities of Cs_xAu (under similar vapor pressure conditions) are one order of magnitude lower and no mixed clusters containing more then one gold atom are detected.

2. Metal–nonmetal transition

Proceeding through the series from LiAu to CsAu, stoichiometric 1:1 alkali–gold compounds exhibit a transition from metallic to nonmetallic behavior. Bulk NaAu is metallic, whereas CsAu is an ionic semiconductor. At the cluster limit, experiments and calculations on Na_xAu clusters indeed point to delocalized *s* valence electrons already for clusters as small as Na_9Au. This jelliumlike behavior is further supported by prominent stability maxima at Na_8Au_2 and $Na_{16}Au_2$ and by the drop of the ionization potentials after the second $(1s,1p,2s)$ and third shell $(1s,1p,1d)$ closings. On the other hand, the experimental data on Cs_xAu disagree with a purely electronic shell model. The computational investigation shows an enhanced ionic interaction already for cesiumaurid clusters consisting of less than 10 atoms.

V. CONCLUSION

A comparative gas-phase study of two sets of mixed metal alkali/gold clusters is presented, supplemented by relativistic density functional calculations on selected model clusters. Experimentally, Na_xAu and Cs_xAu clusters have been generated via supersonic expansions and their relative stabilities as a function of size and ionization potentials have been reported. Data on Na_xAu are interpreted within an electronic shell model. In contrast, the trend in the ionization potentials for Cs_xAu contraindicate considerations based on a shell model alone.

The results of the electronic structure calculations suggest that in Na_xAu clusters the various Na–Au bonds are rather uniform and that the Na–Na interaction is rather strong, while in Cs_xAu clusters the Cs–Au bonds may display large differences, as is expected if CsAu or Cs_2Au subunits are present. In Na_xAu clusters the Na–Au bonding is affected by delocalized electrons which exhibit a somewhat polarized charge distribution with Au being slightly negative. On the other hand, the calculated properties of the Cs_xAu clusters are well described by an ionic bonding model. In general, there is good overall agreement between the theoretical and the experimental observations.

Throughout the discussion, the correspondence between the macroscopic intermetallic compounds and their nanoscopic counterparts has been stressed. In particular, it is suggested that properties of 1:1 sodium–gold alloy and cesiumaurid, like their heat-of-formation, electronic delocalization, and geometric structure, are reflected at the smallest pieces of matter.[33]

ACKNOWLEDGMENTS

The experiments, performed at the University of Bern, were supported by the Swiss National Science Foundation (Grant No. 2.7 2050 178). C.Y. thanks Professor Edward W. Schlag and the Technische Universität München for their hospitality and the Alexander von Humboldt Foundation for a fellowship. M.S., P.G., and N.R. thank Dr. K. M. Neyman for fruitful discussions; M.S. and N.R. are grateful for support from the European Community under the Human Capital and Mobility Programme (Grant No. CHRX-CT94-0532). The work of N.R. is supported by the Deutsche Forschungsgemeinschaft and by the Fonds der Chemischen Industrie.

[1] J. Jortner, Ber. Bunsenges. Phys. Chem. **88**, 188 (1984); T. P. Martin, Angew. Chem. **98**, 197 (1986); M. M. Kappes, Chem. Rev. **88**, 369 (1988).
[2] D. G. Pettifor, in *The Science of New Materials*, edited by A. Briggs, (Blackwell, Oxford, 1992), p. 86, and references therein.
[3] R. Nesper, Angew. Chem. Int. Ed. Engl. **30**, 789 (1991).
[4] J. D. Corbett, Chem. Rev. **85**, 383 (1985).

[5] H. T. J. Reijers, M.-L. Saboungi, D. L. Price, J. W. Richardson, Jr., and K. J. Volin, Phys. Rev. B **40**, 6018 (1989).
[6] A. H. Sommer, Nature **152**, 215 (1943).
[7] W. E. Spicer, A. H. Sommer, and J. G. White, Phys. Rev. **115**, 57 (1959).
[8] F. Hensel, Adv. Phys. **28**, 555 (1979).
[9] G. Kienast and J. Verma, Z. Anorg. Allg. Chem. **310**, 143 (1961).
[10] C. Koenig, N. E. Christensen, and J. Kollar, Phys. Rev. B **29**, 6481 (1984).
[11] W. E. Spicer, Phys. Rev. **125**, 1297 (1962).
[12] A. Hasegawa and M. Watabe, J. Phys. F **7**, 75 (1977); N. E. Christensen and J. Kollar, Solid State Commun. **46**, 727 (1983).
[13] Gold has the highest electron affinity among the metals, 223 kJ mol^{-1}, close to that of iodine (295 kJ mol^{-1}), whereas cesium has the lowest (45.5 kJ mol^{-1}); H. Hotop and W. C. Lineberger, J. Phys. Chem. Ref. Data **4**, 539 (1975). The electron affinity of sodium is 52.9 kJ mol^{-1}.
[14] U. Zachwieja, Z. Anorg. Allg. Chem. **619**, 1095 (1993).
[15] P. Krieger-Beck, A. Brodbeck, and J. Strähle, Z. Naturforsch. **44b**, 237 (1989).
[16] R. J. Batchelor, T. Birchall, and R. C. Burns, Inorg. Chem. **25**, 2009 (1986).
[17] C. Feldmann and M. Jansen, Angew. Chem. Int. Ed. Engl. **32**, 1049 (1993).
[18] M.-L. Saboungi, W. Geertsma, and D. L. Price, Annu. Rev. Phys. Chem. **41**, 207 (1990).
[19] K. Albert, K. M. Neyman, V. A. Nasluzov, S. Ph. Ruzankin, C. Yeretzian, and N. Rösch, Chem. Phys. Lett. **245**, 671 (1995).
[20] U. Heiz and A. Vayloyan, Ph.D. thesis, University of Bern, 1991.
[21] M. M. Kappes, M. Schär, and E. Schumacher, J. Phys. Chem. **91**, 658 (1987).
[22] M. M. Kappes, M. Schär, P. Radi, and E. Schumacher, J. Chem. Phys. **84**, 1863 (1986).
[23] U. Heiz, U. Röthlisberger, A. Vayloyan, and E. Schumacher, Is. J. Chem. **30**, 147 (1990).
[24] C. Yeretzian, J. Phys. Chem. **99**, 123 (1995).
[25] C. Yeretzian, U. Röthlisberger, and E. Schumacher, Chem. Phys. Lett. **237**, 334 (1995).
[26] A. Hermann, E. Schumacher, and L. Wöste, J. Chem. Phys. **68**, 2327 (1978).
[27] M. M. Kappes, R. Kunz, and E. Schumacher, Chem. Phys. Lett. **91**, 413 (1982).
[28] M. M. Kappes, P. Radi, M. Schär, C. Yeretzian, and E. Schumacher, Z. Phys. D **3**, 115 (1986).
[29] P. M. Guyon and J. Berkowitz, J. Chem. Phys. **54**, 1814 (1971).
[30] U. Röthlisberger, M. Schär, and E. Schumacher, Z. Phys. D **13**, 171 (1989).
[31] H. G. Limberger and T. P. Martin, J. Chem. Phys. **90**, 2979 (1989).
[32] M. M. Kappes, M. Schär, U. Röthlisberger, C. Yeretzian, and E. Schumacher, Chem. Phys. Lett. **143**, 251 (1988).
[33] R. L. Whetten, M. R. Zakin, D. M. Cox, D. J. Trevor, and A. Kaldor, J. Chem. Phys. **85**, 1697 (1986).
[34] K. Watanabe, J. Chem. Phys. **22**, 1564 (1954); K. Watanabe and J. R. Mottl, *ibid.* **26**, 1773 (1957); K. Watanabe, *ibid.* **26**, 542 (1957).
[35] C. Bréchignac and Ph. Cahuzac, Chem. Phys. Lett. **117**, 365 (1985).
[36] W. de Heer, Rev. Mod. Phys. **65**, 661 (1993) and references therein.
[37] W. D. Knight, W. A. de Heer, K. Clemenger, and W. A. Saunders, Solid. State Commun. **53**, 445 (1985); C. Bréchignac, Ph. Cahuzac, R. Pflaum, and J.-Ph. Roux, J. Chem. Phys. **88**, 3732 (1988).
[38] K. Clemenger, Ph.D. thesis, University of California, Berkeley, 1985.
[39] W. D. Knight, K. Clemenger, W. A. de Heer, W. A. Saunders, M. Y. Chou, and M. L. Cohen, Phys. Rev. Lett. **52**, 2141 (1984).
[40] M. M. Kappes, P. Radi, M. Schär, and E. Schumacher, Chem. Phys. Lett. **119**, 11 (1985).
[41] M. Brack, Rev. Mod. Phys. **65**, 677 (1993) and references therein.
[42] T. Bergmann, H. Limberger, and T. P. Martin, Phys. Rev. Lett. **60**, 1767 (1988); T. Bergmann and T. P. Martin, J. Chem. Phys. **90**, 2848 (1989).
[43] W. Saunders, Ph.D. thesis, University of California, Berkeley, 1986; W. Saunders, K. Clemenger, W. de Heer, and W. Knight, Phys. Rev. B **32**, 1366 (1985).
[44] C. Yannouleas and U. Landman, Phys. Rev. B **51**, 1902 (1995).
[45] N. Malinowski, H. Schaber, T. Bergmann, and T. P. Martin, Solid State Commun. **69**, 733 (1989).
[46] C. Yeretzian, Diploma thesis, University of Bern, 1986.
[47] M. Kappes, P. Radi, M. Schär, and E. Schumacher, Chem. Phys. Lett. **113**, 243 (1985).
[48] P. Pyykkö and J. P. Desclaux, Acc. Chem. Res. **12**, 276 (1979).
[49] O. D. Häberlen and N. Rösch, Chem. Phys. Lett. **199**, 491 (1992).
[50] B. I. Dunlap and N. Rösch, Adv. Quantum Chem. **21**, 317 (1990).
[51] O. D. Häberlen, S.-C. Chung, and N. Rösch, Int. J. Quantum Chem. Quantum Chem. Symp. **28**, 595 (1994).
[52] O. D. Häberlen, H. Schmidbaur, and N. Rösch, J. Am. Chem. Soc. **116**, 8241 (1994).
[53] S. H. Vosko, L. Wilk, and M. Nusair, Can. J. Phys. **58**, 1200 (1980).
[54] A. D. Becke, Phys. Rev. A **38**, 3098 (1988).
[55] C. Lee, W. Yang, and R. Parr, Phys. Rev. B **37**, 785 (1988).
[56] B. Miehlich, A. Savin, H. Stoll, and H. Preuss, Chem. Phys. Lett. **157**, 200 (1989).
[57] L. Fan and T. Ziegler, J. Chem. Phys. **94**, 6057 (1991).
[58] O. D. Häberlen, Ph.D. thesis, Technische Universität München, 1993.
[59] A. Veillard, Theor. Chim. Acta **12**, 405 (1968).
[60] A. J. Sadlej (private communication).
[61] The atomic radii are 144.2 ppm for gold, 153.7 ppm for sodium and 265.4 ppm for cesium; H. Eccles, *The Periodic Table of Elements Compendium*, edited by C. Clee (The Royal Society of Chemistry, London, 1994).
[62] J. C. Slater, *The Self-Consistent Field for Molecules and Solids: Quantum Theory of Molecules and Solids* (McGraw-Hill, New York, 1974), Vol. 4.
[63] J. F. Janak, Phys. Rev. B **18**, 7165 (1978).